JAMES | Journal of Advances in Modeling Earth Systems

RESEARCH ARTICLE
10.1029/2024MS004535

Precipitation Extremes and Their Modulation by Convective Organization in RCEMIP

Graham L. O'Donnell[1] and **Allison A. Wing**[1]

[1]Department of Earth, Ocean and Atmospheric Science, Florida State University, Tallahassee, FL, USA

Key Points:

- Models in which convection becomes more organized with warming exhibit super-Clausius-Clapeyron growth of precipitation extremes
- Changes in organization correlate with changes in extreme precipitation down to scales as small as 1-hourly and 6-km resolution
- Increases in column-relative humidity in the moist, aggregated region appear likely to modulate these changes in extreme precipitation

Correspondence to:
G. L. O'Donnell,
glodonnell@fsu.edu

Citation:
O'Donnell, G. L., & Wing, A. A. (2024). Precipitation extremes and their modulation by convective organization in RCEMIP. *Journal of Advances in Modeling Earth Systems*, *16*, e2024MS004535. https://doi.org/10.1029/2024MS004535

Received 26 JUN 2024
Accepted 18 OCT 2024

Abstract We examine the influence of convective organization on extreme tropical precipitation events using model simulation data from the Radiative-Convective Equilibrium Model Intercomparison Project (RCEMIP). At a given SST, simulations with convective organization have more intense precipitation extremes than those without it at all scales, including instantaneous precipitation at the grid resolution (3 km). Across large-domain simulations with convective organization, models with explicit convection exhibit better agreement in the response of extreme precipitation rates to warming than those with parameterized convection. Among models with explicit convection, deviations from the Clausius-Clapeyron scaling of precipitation extremes with warming are correlated with changes in organization, especially on large spatiotemporal scales. Though the RCEMIP ensemble is nearly evenly split between CRMs which become more and less organized with warming, most of the models which show increased organization with warming also allow super-CC scaling of precipitation extremes. We also apply an established precipitation extremes scaling to understand changes in the extreme condensation events leading to extreme precipitation. Increased organization leads to greater increases in precipitation extremes by enhancing both the dynamic and implied efficiency contributions. We link these contributions to environmental variables modified by the presence of organization and suggest that increases in moisture in the aggregated region may be responsible for enhancing both convective updraft area fraction and precipitation efficiency. By leveraging a controlled intercomparison of models with both explicit and parameterized convection, this work provides strong evidence for the amplification of tropical precipitation extremes and their response to warming by convective organization.

Plain Language Summary Organization of tropical clouds into clusters has profound effects on Earth's climate. We examine the impact of this organization on heavy rain events. Across an ensemble of high-resolution computer simulations of an idealized tropical atmosphere, we find that when storms become more clustered with warming, the heaviest rainfall events increase by more than expected. This work shows the importance of accurately modeling the changes in organization with warming as well as the importance of running computer models with a fine enough resolution to capture individual storms.

1. Introduction

1.1. Motivation and Background

Convective organization is well-established as a major element of the tropical climate (Muller & Takayabu, 2020; Pendergrass, 2020). A more organized scene leads to profound changes in the atmospheric state, including a net warming and drying in the mean state while a moister convecting region forms (Wing, 2019). These changes cause an increase in mean precipitation, as the drier region cools more efficiently, requiring more convection to maintain a state of radiative-convective equilibrium (RCE) (e.g., Allen & Ingram, 2002). Unlike the mean state, extreme precipitation is not constrained by energetics. Extreme precipitation's response to warming is thus more uncertain, particularly in the tropics (O'Gorman & Schneider, 2009a) where other factors such as moisture availability, updraft vertical mass flux, and microphysics control it (O'Gorman & Schneider, 2009a; see also Muller et al., 2011). Cloud-resolving model (CRM) simulations of RCE broadly support a thermodynamic scaling with lower-tropospheric humidity (Abbott et al., 2020; Muller & Takayabu, 2020; Muller et al., 2011; Romps, 2011). Departures from thermodynamics may occur (Singh & O'Gorman, 2013; Westra et al., 2014), and have been linked to changes in updrafts (O'Gorman, 2015). As tropical precipitation extremes are observed to be frequently produced by organized features (e.g., Dai & Soden, 2020; Hamada et al., 2014; Nesbitt et al., 2006; Roca & Fiolleau, 2020; Semie & Bony, 2020), recent work has examined the link between tropical extreme precipitation and convective organization and how this link may change in a warming climate.

Many studies have examined the link between extreme precipitation and convective organization in model simulations under a wide variety of circumstances. Changes in extreme precipitation have been linked to changes in organization modulated by changing domain size alone (e.g., Da Silva et al., 2021), sea surface temperature (SST) (Pendergrass et al., 2016), shear (Abramian et al., 2023; Muller, 2013), radiative effects (e.g., Bao & Sherwood, 2019; Fildier et al., 2021), surface fluxes (Fildier et al., 2021), convective parameterizations, large-scale circulations, resolution (Bao et al., 2017), and storm size (Bao et al., 2024). Most such papers find increases in extreme rainfall with increased organization and/or a super-Clausius-Clapeyron (super-CC) increase in extreme rainfall with warming when the system becomes more organized. Previous work on the topic has examined either a single model or ensembles of GCMs, in either an RCE state or using an AMIP configuration (e.g., Li et al., 2022; Medeiros et al., 2021; O'Gorman, 2012; O'Gorman & Schneider, 2009a). This paper is the first to examine the relationship between changes in extreme precipitation and convective organization across an ensemble of cloud-resolving models. Resolving convection is critical to realistically representing certain organized features in the tropics (e.g., Rios-Berrios et al., 2022), so this is an important step in advancing our understanding of extreme rainfall events. We also note that previous work on extreme tropical rainfall used a variety of definitions of "extreme," with a range of percentiles from the 99th to the 99.99th and beyond, timescales from instantaneous to daily, and spatial scales from CRM grid resolutions to hundreds of kilometers. Perhaps because of this wide range of methodologies and the variety of models used, these prior studies disagree on the physical mechanisms responsible for the relationship between convective organization and extreme precipitation, such as whether the link is modulated primarily via properties of updrafts (a dynamic contribution) or via precipitation efficiency. The dynamic term shows wide variation across studies. Pendergrass et al. (2016) find a massive 60%/K contribution from updraft magnitude across the boundary between SSTs that lead to aggregation and those that do not. Fildier et al. (2021) find a much smaller 12%/K contribution in the same situation. In both studies, changes in precipitation extremes are much smaller when there are not large changes to the degree of organization. Definitions of precipitation efficiency can also vary. Lutsko and Cronin (2018) find that precipitation efficiency decreases with increased organization (though not enough to counteract its increases with warming) while Fildier et al. (2021) suggest efficiency is modulated by the humidity of the region where precipitation falls. Authors also disagree on whether there is any effect of organization on instantaneous rain rates. Da Silva et al. (2021) found a 30% increase in rain rates due to the presence of organization, caused by a +50% microphysical contribution and a −25% dynamic contribution. By contrast, Bao and Sherwood (2019) found instantaneous precipitation showed little change, caused by offsetting decreased dynamic contribution and increased efficiency. By applying a common methodology across the model ensemble, we seek to resolve these disagreements and more firmly establish the link between extreme precipitation and organization.

1.2. RCEMIP

The Radiative-Convective Equilibrium Model Intercomparison Project (RCEMIP) (Wing et al., 2018, 2020a) provides a controlled framework to examine the properties of convective organization across models. Many models- including cloud-resolving models (CRMs), general circulation models (GCMs), large eddy simulation models (LES), and global cloud-resolving models (GCRMs)- took part in RCEMIP. Each model was run with a common framework representative of the tropical atmosphere. No rotation and no diurnal cycle of solar radiation were used, and each model was run with a fixed and uniform SST of 295, 300, and 305 K. Each simulation was allowed to evolve to an RCE state. However, each model used its own microphysical and radiation schemes: common results across RCEMIP are thus likely to be robust to such parameterizations. RCEMIP is the first model intercomparison of the RCE state involving CRMs and thus the first to include storm-scale dynamics.

RCEMIP was designed to examine the effect of convective organization, and for this purpose models were run on two domain sizes: a large domain allowing convective self-aggregation and a small domain too confined to support it. The organized nature of the large-domain simulations causes notable changes to the atmospheric structure, including a net drying and warming. Although the RCE state varies between models, the mean precipitation across the large-domain simulations is larger than that across the small-domain simulations because of enhanced radiative cooling in dry regions (Wing et al., 2020a). Although the wide spread in the degree of organization and its response to warming makes it difficult to understand what sets the degree of organization, this spread allows examination of how the degree of organization modifies other climate properties. For example, organization has been shown to be an important factor in setting climate sensitivity, where the GCMs typically have a lower climate sensitivity than CRMs in part because the GCMs show increased organization with warming

(Becker & Wing, 2020). In this paper, we examine how organization and its changes with warming impact extreme precipitation and its changes with warming.

1.3. Objectives

Our objectives in performing this study include:

1. Assessing the impact of the existence, degree, and changes with warming of convective organization on extreme precipitation
2. Systematically evaluating the spatiotemporal scales at which precipitation extremes are impacted by domain-wide convective organization
3. Testing the applicability of an established scaling for precipitation extremes across a large ensemble of models with explicit convection
4. Establishing physical mechanisms linking organization and extreme precipitation

2. Methods

2.1. O'Gorman and Schneider (2009a) Scaling

O'Gorman and Schneider (2009a) separated changes in extreme precipitation into components caused by dynamic and thermodynamic changes by using a scaling comparing precipitation to the condensation that occurs to balance it. To maintain the atmosphere at saturation during an extreme precipitation event, the precipitation rate P must be balanced by the vertically integrated condensation rate C. At hot or cold SST denoted by subscripts h or c, respectively, P and C are given by

$$P_{h,c} \approx C_{h,c} = \int c_{h,c} dp = \int -\omega_{h,c} \left(\frac{dq_s}{dp} \right) \Big|_{\theta^*;h,c} dp \tag{1}$$

The condensation rate at a point is given by the product of vertical velocity (ω) and the vertical derivative of saturation specific humidity along a moist adiabat at the local temperature and pressure $\left(\left(\frac{dq_s}{dp} \right) \Big|_{\theta^*;h,c} \right)$. Muller et al. (2011) pointed out that not all of this condensation precipitates, so they added a precipitation efficiency factor ϵ outside the integral.

The dynamic term is found by isolating changes caused solely by changes in the updrafts, including changes in updraft height, area, and strength. The thermodynamic term is found by isolating changes caused solely by differences in the temperature structure of the atmosphere at two different sea surface temperatures. Letting angled brackets denote an SST-averaged vertical profile, we calculate the dynamic condensation integrals as

$$D_{h,c} = \int -\omega_{h,c} \left\langle \frac{dq_s}{dp} \right\rangle dp \tag{2}$$

and the thermodynamic integrals as

$$Q_{h,c} = \int -\langle \omega \rangle \left(\frac{dq_s}{dp} \right)_{h,c} dp. \tag{3}$$

For a given term X in the scaling, let X_h represent the value at a warm temperature and X_c be the value at a cold temperature. We choose to calculate the change in X as a function of the sea surface temperature T arithmetically as a percentage of the average condensation rate. This is consistent with Muller et al. (2011) but modified to work well over a large temperature difference. Using ΔX as a shorthand:

$$\Delta X = \frac{dX}{dT} = \frac{1}{\Delta T} \frac{X_h - X_c}{\frac{C_h + C_c}{2}} \tag{4}$$

The only exception is the change in precipitation, for which the denominator is the average value of extreme precipitation:

$$\Delta P = \frac{dP}{dT} = \frac{1}{\Delta T}\frac{P_h - P_c}{\frac{P_h + P_c}{2}} \tag{5}$$

Equations 2 and 3 are used to calculate the dynamic (ΔD) and thermodynamic (ΔQ) components of the change in precipitation with warming as in Equation 4. The full scaling is given as the condensation rate by Equation 1. Notice that by using the common denominator of $\frac{C_h + C_c}{2}$ in Equation 4, we find $\Delta C = \Delta D + \Delta Q$; there is no nonlinearity between these three terms. We then calculate the efficiency term as a residual:

$$\Delta E = \Delta P - \Delta C \tag{6}$$

This term includes any other factor impacting the amount of precipitation. This clearly includes the actual precipitation efficiency (including changes in horizontal convergence of condensate, detrainment, storage, and re-evaporation) as well as any other inaccuracies in the relationship between the scaling and true condensation.

In addition to Equation 4, we tested two alternative calculations based on geometric rates of change, that is, $\Delta X = \frac{1}{\Delta T}\ln\frac{X_h}{X_c}$. Results were qualitatively similar, so we chose to use Equation 4 for the remainder of the paper. Quantitatively, Equation 4 results in smaller calculated rates of change than the geometric rate of change calculation. If both C_h and C_c are positive, Equation 4 is capped at 20%/K for a 10 K interval. One side effect of this is that any outliers are tempered, reducing their impact on our correlations. For rates of change under 10%/K (exhibited by most models, especially CRMs), the two methods give results within 1%/K.

By definition, Equation 4 results in no non-linearity, although coupled changes between the thermodynamic and dynamic terms may exist in reality. In practice, this nonlinearity is small: less than 1%/K when using geometric scaling calculations. We can thus safely ignore it in this analysis.

2.1.1. Dynamic Magnitude and Shape Separation

We further separate the dynamic term into contributions from updraft magnitude and shape. Defining the temperature-averaged updraft structure $\langle\omega\rangle = \frac{\omega_h + \omega_c}{2}$, we can express ω_h in terms of some factor times this standard profile plus a difference term $\delta\omega$ that comes only from the shape of the vertical profile:

$$\omega_h = m_h\langle\omega\rangle + \delta\omega \tag{7}$$

We define

$$m_h = \frac{\int \omega_h dp}{\int \langle\omega\rangle dp} \tag{8}$$

which implies $\int \delta\omega dp = 0$; $\delta\omega$ includes no component of the updraft magnitude. Defining the magnitude condensation integrals as

$$M_{h,c} = m_{h,c}\int \langle\omega\rangle\left\langle\frac{dq_s}{dp}\right\rangle dp, \tag{9}$$

we then define the dynamic magnitude sub-component ΔM similarly to the other components using Equation 4. The shape sub-component ΔH is calculated as the residual of the dynamic component:

$$\Delta H = \Delta D - \Delta M \tag{10}$$

We carefully choose the word "magnitude" here as ΔM still refers to the combined contribution of changes in updraft strength, the number of convective cells, and the size of each cell. When examining ΔM on the model grid resolution, a single updraft always fills the entire box, so there is no meaningful updraft size contribution. However, most of our results examine coarsened data. A coarser box experiencing extreme precipitation can include strong convective updrafts and downdrafts as well as weaker motions, so while a positive ΔM implies that

updrafts either strengthen with warming or cover a larger fraction of the area, it does not imply each statement individually. We explore this further in Section 5.3.

2.2. Characteristics of RCEMIP Models

In RCEMIP, models were run on two domain sizes. The small domain was an approximately 100×100 km^2 grid at 1-km resolution for CRMs and a single-column configuration for GCMs. The large domain was a long channel of about 6000×400 km^2 at 3-km resolution for CRMs, and an Earth-radius aquaplanet at roughly 1° resolution for most GCMs.

Although the RCEMIP data set includes simulations from many models, not all of them are suitable for this analysis. For a large-domain model to be useful here, it must contain all of the needed data fields (at minimum this includes the hourly averaged two-dimensional precipitation field, returned once every hour as well as the instantaneous three-dimensional temperature, pressure, specific or relative humidity, and vertical velocity, which are returned once every 6 hr). We further exclude the GCRMs as they include so much data that it would have been too computationally intensive to analyze them. This leaves 21 models for analysis, given in Table 1.

2.3. General Procedures

As we find below in Section 3.2, changes in organization and extreme precipitation are correlated over a wide range of spatial and temporal scales. However, they do not significantly correlate at the 3-km base resolution of the CRMs on 1-hourly timescales. An ideal scale for the analysis would coarsen the CRM data enough to find significant relationships but remain fine enough to observe robust statistics of the low-probability extreme precipitation events. While we evaluate the relationship between organization and extreme precipitation and their changes with warming across a wide variety of spatiotemporal scales in Section 4.2, for our application of the O'Gorman and Schneider (2009a) scaling, we choose to spatially coarsen the CRM data to 15-km resolution while keeping the 1-hr timescale. This leaves $O(10^3)$ extreme precipitation events at or above the 99.9$^{\text{th}}$ percentile for each model run. This 15-km scale is sufficient to reach a strong correlation between the changes in organization and extreme precipitation. The GCMs were run at a coarser resolution of approximately 1° (~100 km), so no additional coarsening is required to see correlations between changes in organization and extreme rainfall in these models. Note that although CRM and GCM results are frequently plotted in the same figures in this paper, analyses are generally not performed at the same spatial resolution.

In their analysis, O'Gorman and Schneider (2009a) examined daily precipitation. Here, when applying the scaling we instead examine hourly precipitation. We examine the scaling by compositing the 3-D data fields conditional on extreme values of 2-D precipitation. If we calculate these profiles at the same time as the extreme rainfall, we find no significant correlation between the changes in the scaling and changes in precipitation extremes. The 2-D precipitation field represents the hourly precipitation ending at the given timestamp in most of the RCEMIP models, at a time when convective downdrafts may be occurring. As we implemented the scaling in a way that does not filter out downdrafts, this results in a possibility of a negative scaling. This occurs in some model runs: in three CRMs, the scaling flips sign between the 295 and 305 K runs. To avoid this problem, note that the scaling is designed around near-equilibrium of condensation and precipitation, suggesting an alternative: using 3-D data conditioned on extreme precipitation occurring over the *following* hour. Physically, this follows from how condensation must precede precipitation: although this was not an issue for the daily timescale of O'Gorman and Schneider, our 1-hr timescale is too close to the lifetime of storms to ignore this delay in precipitation. When we perform this, we find a significant correlation between changes in the time-shifted scaling and extreme precipitation with warming across the CRMs ($r = 0.87$ with the shift, $r = 0.47$ without it), elaborated on in Section 5.1. Although a strong correlation exists between these variables for GCMs even without the shift ($r = 0.98$ with the shift, $r = 0.99$ without it), we chose to shift the GCM data as well for consistency in our methodology. An alternative method would be to calculate the scaling at every model gridpoint and then composite over extreme condensation events (as in Da Silva et al. (2021)), but this is much more computationally expensive for the large ensemble of RCEMIP.

We generally choose to average over all events at or above a given percentile of extreme precipitation. This is a fairly common technique when working with the scaling to improve statistics; this exact procedure was performed by Muller et al. (2011). In all sections of this paper involving correlations (Section 3.2 and all sections including and after Section 4.2) we also average the precipitation over all events at or above the percentile. In other sections

Table 1
All the Models Used in This Work

Abbreviation	Name	Model type	Domains
CAM5-GCM	Community Atmosphere Model v5	GCM	L
CAM6-GCM	Community Atmosphere Model v6	GCM	L
CM1	Cloud Model 1, cm1r19.6	CRM/LES	L/S
CNRM-CM6	Atmospheric component of the CNRM Climate Model 6.1	GCM	L
DALES	Dutch Atmospheric Large-Eddy Simulation model v4.2	CRM/LES	S
DAM	Das Atmosphaerische Modell	CRM	L/S
ECHAM6-GCM	MPI-M Earth System Model-Atmosphere component v6.3.04p1	GCM	L
FV3	GFDL-FV3CRM	CRM	L/S
GEOS-GCM	Goddard Earth Observing System model v5.21	GCM	L
ICON-GCM	ICOsahedral Nonhydrostatic Earth System Model-Atmosphere component	GCM	L
ICON-LEM-CRM	ICOsahedral Nonhydrostatic-2.3.00, LEM config.	CRM	L/S
ICON-NWP-CRM	ICOsahedral Nonhydrostatic-2.3.00, NWP config.	CRM	L/S
IPSL-CM6	IPSL-CM6A-LR	GCM	L
MESONH	Meso-NH v5.4.1	CRM/LES	L/S
MicroHH	MicroHH v2.0	CRM/LES	S
SAM-CRM	System for Atmospheric Modeling 6.11.2	CRM/LES	L/S
SAM0-UNICON	Seoul National University Atmosphere Model v0	GCM	L
SCALE	SCALE v5.2.5	CRM	L/S
SP-CAM	Super-Parameterized Community Atmosphere Model	GCM	L
SPX-CAM	Multi-instance Super-Parameterized CAM	GCM	L
UCLA-CRM	UCLA Large-Eddy Simulation model	CRM	L/S
UKMO-CASIM	UK Met Office Idealized Model v11.0—CASIM	CRM	L/S
UKMO-GA7.1	UK Met Office Unified Model Global Atmosphere v7.1	GCM	L
UKMO-RA1-T	UK Met Office Idealized Model v11.0—RA1-T	CRM	L/S
UKMO-RA1-T-hrad	UK Met Office Idealized Model v11.0—RA1-T (homogenized radiation)	CRM	L/S
UKMO-RA1-T-nc	UK Met Office Idealized Model v11.0—RA1-T (no cloud parameterization)	CRM	L/S
WRF-COL-CRM	Weather Research and Forecasting model v3.5.1	CRM	L/S
WRF-CRM	Weather Research and Forecasting model v3.9.1	CRM	L/S

Note. Italicized names are excluded from correlation analysis and are only used in Figures 1, 2, and 4. L and S indicate the large and small domains, respectively.

we only use the threshold value for extreme precipitation. As for which percentile to use to identify extreme precipitation, we consider a variety of different high percentiles when considering the difference in extreme precipitation between the small and large simulations in Section 3.1 and when considering the response of precipitation to warming in Section 4.1, but focus on one high percentile for the rest of the analysis. The 99.9th-percentile seems to be a middle ground across studies, with some using either a higher (e.g., 99.99th by Singh and O'Gorman (2014)) or lower (e.g., 99th by Pendergrass et al. (2016)) percentile. Higher percentiles seem to be more often used on shorter, smaller timescales, so we usually checked results for both the 99.9th and 99.99th percentile. Results were typically similar, so we show only the 99.9th-percentile results here. We calculate these percentiles as a function of all hours, not just rainy hours, following a convention set by O'Gorman and Schneider (2009a) and many other works cited in this paper. This avoids any issues related to changing precipitating fraction with warming (Schär et al., 2016) as well as any cross-model differences in handling immeasurably small but positive rainfall amounts.

2.4. Quantification of Convective Organization

To compare the degree of organization across models, we utilize the three metrics computed by Wing et al. (2020a): organization index (I_{org}; Tompkins & Semie, 2017), subsidence fraction (SF), and variance of column relative humidity (V). Higher values of each denote more strongly organized convection. We choose to focus our analysis on I_{org}, as it most directly represents the spatial clustering of convection. Its values range from 0 to 1, where a value of 0 represents regularly spaced convection, 0.5 represents random convection, and 1 represents fully organized convection. In RCEMIP, the convective cells used to calculate I_{org} were identified by using a threshold of OLR. Changes in I_{org} show the strongest correlation with changes in extreme precipitation across models. Larger SF also correlates with larger precipitation extremes. Large V does not significantly correlate with extreme precipitation across models, perhaps because it represents an environmental response to clustered convection rather than representing the clustering itself. It may thus be susceptible to how each model represents the environment's base state, seen as a proportionally larger cross-model spread in V compared to the other metrics (Wing et al., 2020a).

3. Extreme Precipitation and Organization

3.1. Characteristics of Extreme Precipitation in RCEMIP

Although most of this paper focuses on how the varying degree of organization across the large-domain simulations impacts the rate of increase of extreme precipitation with warming, we can gain some insight into how the presence of organization impacts extreme rainfall by comparing the large- and small-domain simulations. As the large domain allows organization while the small domain prohibits it, differences between the two can be caused by the presence or absence of organized convection. Figure 1 shows the hourly precipitation rate as a function of percentile for each model of the RCEMIP ensemble, when the CRM data are coarsened to 15 km and the GCM data are left at the default resolution. Solid lines represent CRMs, while dashed lines represent GCMs. Above roughly the 99th percentile, the large domain simulations show dramatically higher rain rates than the small domain. $P_{99.9}$ is greater than 5 mm/hr in nearly every large-domain CRM, while the same CRMs show rain rates below 5 mm/hr in the small domain. The exceptions, in the DALES model family, do not have corresponding large-domain simulations. Extreme precipitation in the GCMs tends to converge toward rain rates of around 10 mm/hr in the highest percentiles in the large domain. Extremes are not shown for GCMs in the small domain, as the single-column model setup cannot meaningfully simulate local extreme precipitation.

Figure 2 highlights this difference by showing the ratio of large-domain to small-domain rainfall at a given percentile. The gray dashed line shows a ratio of 1: values above this line imply that the large domain shows larger rain rates. At low percentiles, precipitation rates in the small domain exceed that of the large domain, reflecting how the organized large-domain simulations spontaneously form large dry regions. However, above around the 99th percentile, precipitation in the large-domain simulations dramatically exceeds the corresponding small domain simulations. Although this is partially due to poor statistics in the small domain simulations (with this coarsening, values above the 99.9th percentile are defined by less than 10 events), large-domain hourly rain rates exceed small domain rain rates at the highest percentiles in most models even at their native resolutions (not shown), despite the expectation that large-domain grid cells should smooth out some extremes due to the larger area. When the small-domain data are coarsened to 3-km resolution to match the large-domain simulations, every model's extreme rain rates are more intense in the large domain. This may be connected to the observation by Parodi and Emanuel (2009) that modeled extreme updrafts are weaker when cramped into a smaller domain, even when only comparing domains too small to support organization. This enhancement of rainfall is also seen with instantaneous rates as approximated by lowest-level precipitating liquid water content, which is consistent with the results of Da Silva et al. (2021). Thus, the presence of organization appears sufficient to increase extreme precipitation rates. The effect is larger when examined over a larger area, although it is unclear how much of this effect is due to the enhancement of extreme precipitation due to organization and how much is instead caused by the limited sample size in the small domain simulations. We also cannot rule out model resolution as a factor: although not as universal as the comparison between large and small-domain simulations, a comparison of the six model families with both a standard small-domain simulation and an LES simulation shows that even with the same domain size, a majority of models show decreased 1 and 3-km extreme precipitation with the finer LES resolution.

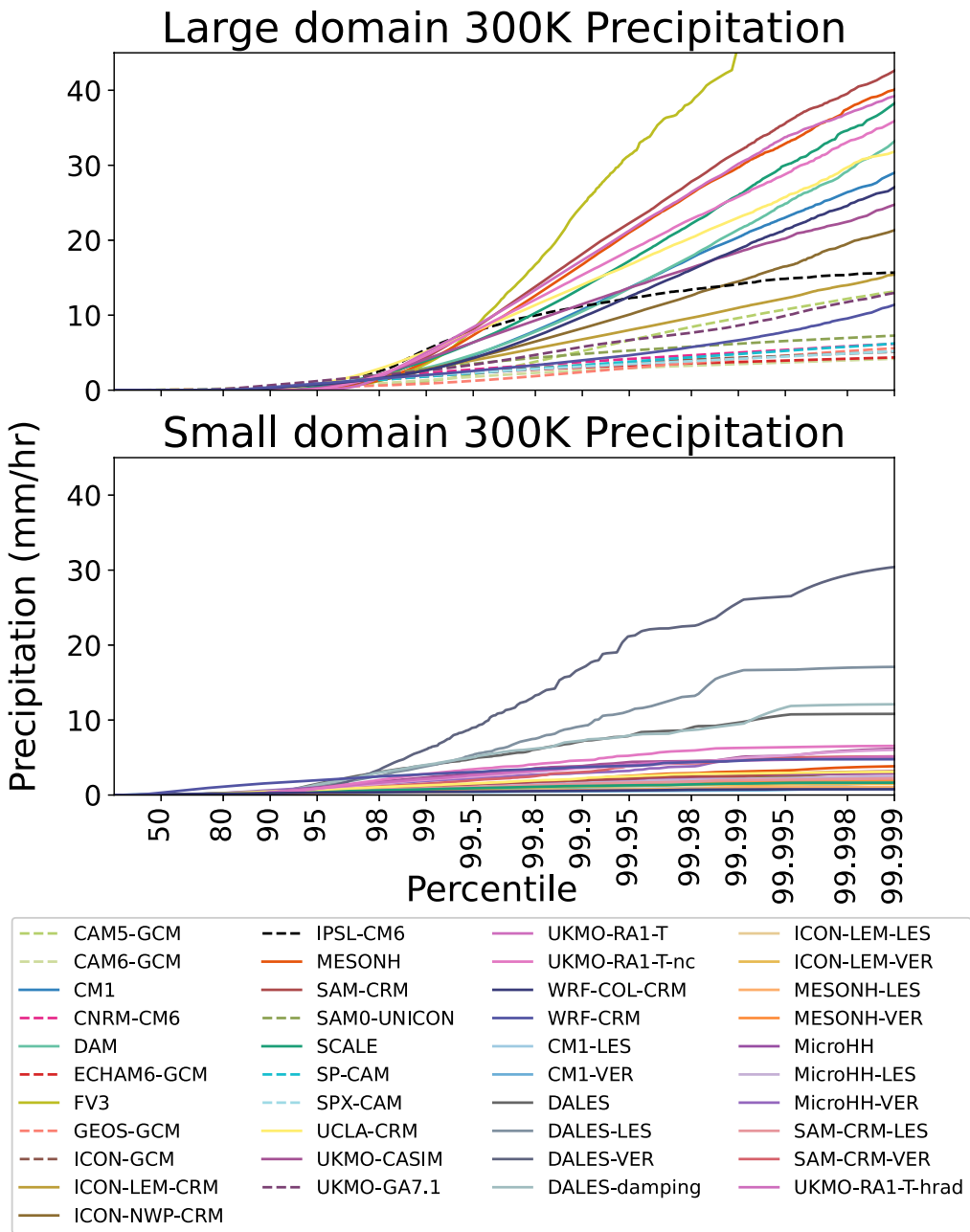

Figure 1. Values of extreme hourly precipitation by model and percentile, with CRM data coarsened to 15 km. CRMs are represented by solid lines and GCMs are represented by dashed lines.

3.2. Correlations Between Extreme Precipitation and Organization Index

Across the CRMs of RCEMIP, extreme precipitation correlates with I_{org} when the data are sufficiently coarsened. Figure 3 shows the correlation coefficients of $P_{99.9}$ against I_{org} for the 300 K large-domain CRMs used in this analysis over a wide range of spatiotemporal scales. While no significant correlations exist at the 1-hr, 3-km grid scale, coarsening in space quickly causes correlations to appear. At 30 km it reaches statistical significance with $p < 0.01$. The strongest correlation appears for 12–24-hr precipitation at 90 km resolution. We find no significant correlations between $P_{99.9}$ and I_{org} at instantaneous timescales at any spatial scale. This map of correlation coefficients is robust when instead examining the 99.99th percentile.

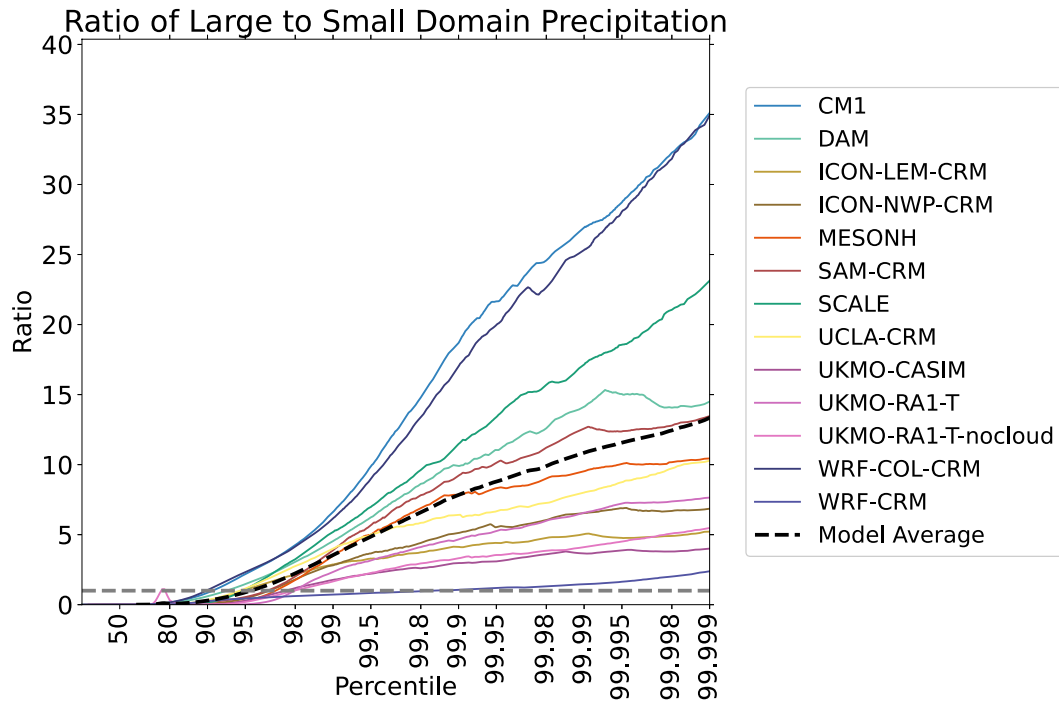

Figure 2. Ratio between 1-hourly, 15 km extreme precipitation of a given percentile between the large and small domain simulations at 300 K. The black dashed line is the multi-model average, and the gray dashed line is a ratio of 1.

4. Changes in Extreme Precipitation and Changes in Organization

4.1. Change of Precipitation With Warming in the Large-Domain Simulations

Figure 4 shows the rate of change of extreme 15-km hourly precipitation with SST warming between the coolest and warmest simulations in the large-domain models. Though the intermodel spread is large, all but one show an increase in extreme precipitation. The sole exception, WRF-CRM, is noted by Wing et al. (2020a) as the only model to include a disorganized large-domain simulation at 300 K as well as the model with the largest decrease in

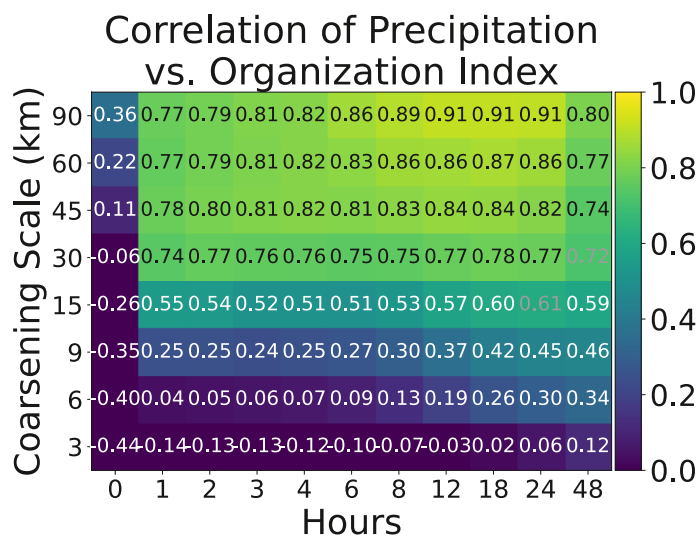

Figure 3. Correlation coefficients between the values of extreme precipitation (defined as precipitation averaged above the 99.9th percentile) and organization index across the 300 K large-domain CRM simulations. Black text denotes a p-value less than 0.01, and gray text denotes a p-value less than 0.05.

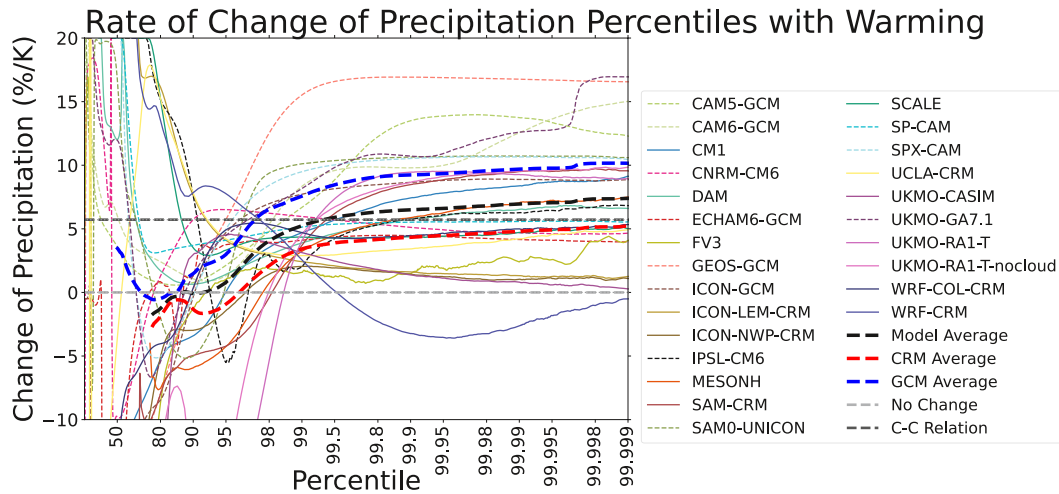

Figure 4. Rate of change of 1-hourly, 15-km precipitation percentiles with warming in each large-domain model of the RCEMIP ensemble. These rates of change are calculated between 295 and 305 K.

organization index with warming between 295 and 305 K. The only other CRM simulation with $I_{org} < 0.5$ is UKMO-CASIM's 305 K simulation, and this model is seen to have the slowest increase in extreme precipitation with warming.

Importantly, we see that most models approach constant rates of change as a function of percentile. This allows us to define an extreme regime beginning around the 99.8th percentile, within which we should expect similar results no matter what percentile we choose to examine. We chose to work primarily with the 99.9th percentile for the maximum number of extreme precipitation events, though most results also hold at the 99.99th percentile.

Fildier et al. (2017) showed that in a comparison between a GCM setup and superparameterized convection, resolved convection allows convergence of the change in rain rates with warming closer to the Clausius-Clapeyron (CC) relation, an observation which is supported by Figure 4. In our work, CRMs (solid lines) and GCMs (dashed) are distinguished by their intermodel spread and their average rates of change in precipitation with warming. GCMs show faster increases in extreme precipitation with warming and a wider spread in results. CRMs are more confined to smaller rates of change, and the CRM average in the extreme regime is remarkably close to the Clausius-Clapeyron relation with respect to surface temperature. The following sections focus on why this Clausius-Clapeyron scaling holds and on how the intermodel spread is related to organization.

4.2. Correlations Between Changes in Extreme Precipitation and Organization

Figure 3 demonstrated that extreme rainfall can be linked to organization. We can more strongly link changes in these two variables with warming by correlating $\Delta P_{99.9}$ against ΔI_{org}. While there is again no significant correlation at the native data resolution of 3 km, coarsening by just a factor of 2 in space is sufficient for significance at the p = 0.05 level (Figure 5b). As demonstrated in Figure 5a, correlations between changes in organization and changes in extreme precipitation appear in both CRMs and GCMs. Both regression lines also pass close to the point where no change in organization would correspond to a Clausius-Clapeyron scaling in extreme precipitation. Among the CRMs, which are nearly evenly split between increasing and decreasing organization, the majority of those which become more organized also show super-CC increases in extreme precipitation and vice versa. Most of the GCMs show increases in organization, and as such most of them also show super-CC increases in extreme precipitation with warming. Thus, the behavior of organization appears to play a large role in whether and how a model deviates from CC scaling.

In a comparison between Figures 3 and 5b, it is reasonable to expect stronger correlations between changes in organization and changes in extreme precipitation than between the values of each. Comparisons of the values themselves depends heavily on model properties impacting the base state and base rain rates, while examining changes in extreme rain rates within a given model should cancel out some of the cross-model variability in the base state.

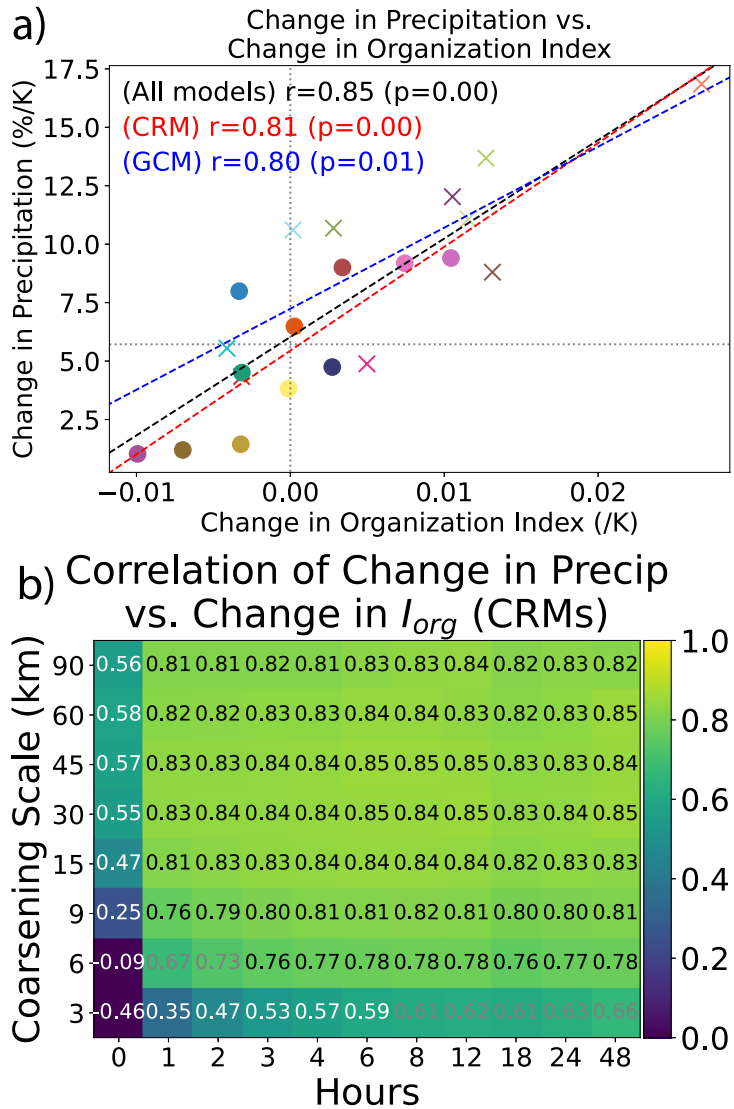

Figure 5. (a) Change in 99.9th-percentile precipitation (defined by averaging all events at or above this percentile) at 1-hourly, 15-km scale versus the change in organization index across the large-domain simulations, as calculated between the 295 and 305 K simulations. Each circle represents a CRM within the ensemble, while each cross represents a GCM. The vertical dotted line marks no change in the degree of organization while the horizontal dotted line shows the Clausius-Clapeyron rate. (b) Correlation coefficients between the changes in 99.9th-percentile precipitation and organization index across CRMs at various spatiotemporal scales. Black text denotes a p-value less than 0.01, and gray text denotes a p-value less than 0.05.

Significance in these correlations remains when extreme precipitation is correlated against subsidence fraction instead of organization index, although the exact spatiotemporal scales required for correlations change somewhat. SF and $P_{99.9}$ correlate significantly down to smaller length scales, with similar maximum correlation coefficients. Most of the correlations between ΔSF and ΔP are slightly weaker than those between ΔI_{org} and ΔP, although the correlations at instantaneous time scales just reach significance at length scales of at least 30 km. While correlations remain between $P_{99.9}$ and CRH variance at coarser and longer-duration scales, correlations involving the changes of these variables are lost (not shown).

The correlation coefficients here justify our choice of primarily using 1-hourly, 15-km precipitation extremes. This scale is large enough to show relevant correlations between organization and extreme precipitation: if a link exists, it should be found here. This agrees with Fildier et al. (2017), who found a difference in the response to organization between the mesoscale and convective scale: extreme mesoscale precipitation shows a stronger response to warming. This 15 km scale is still fine enough that we have a large number of samples of extreme

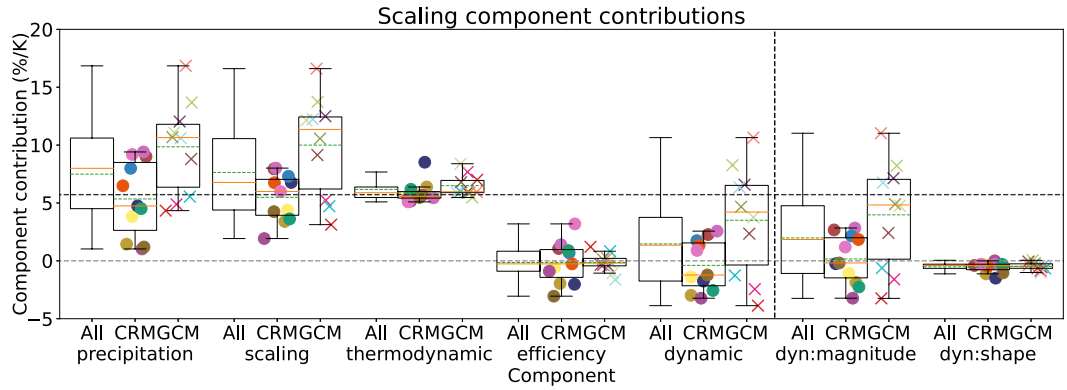

Figure 6. Scaling components for 1-hourly, 15-km precipitation for the large-domain models. Components are calculated between 295 and 305 K. Each circle represents a CRM while each cross represents a GCM. The boxes-and-whiskers show the cross-model spreads for all models (left), CRMs (center), and GCMs (right). The solid orange lines show the multi-model mean values, while the dashed green lines show the median.

precipitation. Each large-domain CRM has over 2000 events exceeding the 99.9$^{\text{th}}$-percentile threshold on this scale.

5. Using the Scaling

5.1. Values of the Scaling Components in RCEMIP

Figure 6 shows the spread in each component for each model, separated into CRMs and GCMs. Several key takeaways are clear. Scaling and precipitation show similar spread, and the scaling does a good job of predicting extreme precipitation (ΔC and ΔP correlate across models with r = 0.87 for CRMs and r = 0.98 for GCMs) (not shown).

The near-Clausius-Clapeyron growth in precipitation extremes is driven by the thermodynamic component, as shown by the tight cluster of almost all CRMs. The most notable outlier from this cluster is WRF-COL-CRM. The key contributor to the thermodynamic component's value is the Clausius-Clapeyron relation, shown by the tight cluster of models around this value. Within the thermodynamic component, the main source of spread is the vertical structure of the updrafts leading to extreme precipitation: maximum updrafts higher in the atmosphere experience super-CC increases in the local saturation specific humidity lapse rate caused by the increased warming in the upper atmosphere along a shifted moist adiabat due to upper-tropospheric amplification (O'Gorman & Schneider, 2009b). When considering the mass-weighted updraft pressure (calculated as $\bar{p} = \frac{\int \rho\omega p dp}{\int \rho\omega dp}$), WRF-COL-CRM is the sole CRM with $\bar{p}$ below 400 hPa: all other CRMs fall between 510 and 620 hPa, with 8 of the 11 CRMs studied falling between 570 and 620 hPa. The correlation between ΔQ and $\bar{p}$ has r = −0.95 across CRMs and r = −0.87 across GCMs. GCMs show a slightly higher thermodynamic contribution, in part because their updrafts occur slightly higher in the atmosphere; all but one have $\bar{p}$ between 520 and 575 hPa. As noted by O'Gorman and Schneider (2009a), when changes to the updraft structure are small, the scaling can be simplified to a measure of updraft velocity times the near-surface saturated water vapor content, a value which scales as the Clausius-Clapeyron relation. This is physically supported by Abbott et al. (2020), who found that variations in updraft structure generally collapse to a common profile when examined as a function of a moisture-based vertical coordinate in an aggregation-permitting CRM.

Dynamics and efficiency contribute to the intermodel spread in ΔP. Both terms are important in the CRMs, while the dynamic term is far more important in GCMs. At the ∼1° resolution of RCEMIP's GCMs, we found that the fraction of extreme precipitation produced by the convective parameterization is large (not shown). This precipitation can instantly fall out without experiencing the moister atmosphere of the aggregated region, resulting in no link between the precipitation efficiency component and organization. Although not shown, further coarsening of the CRMs (e.g., to 60 km) reduces the spread in efficiency but increases the spread in the dynamic contribution. Other studies have found that running GCMs at finer scales causes them to rely less on their convective parameterization to produce extreme rainfall (Nikumbh et al., 2024; Terai et al., 2018), which may allow the

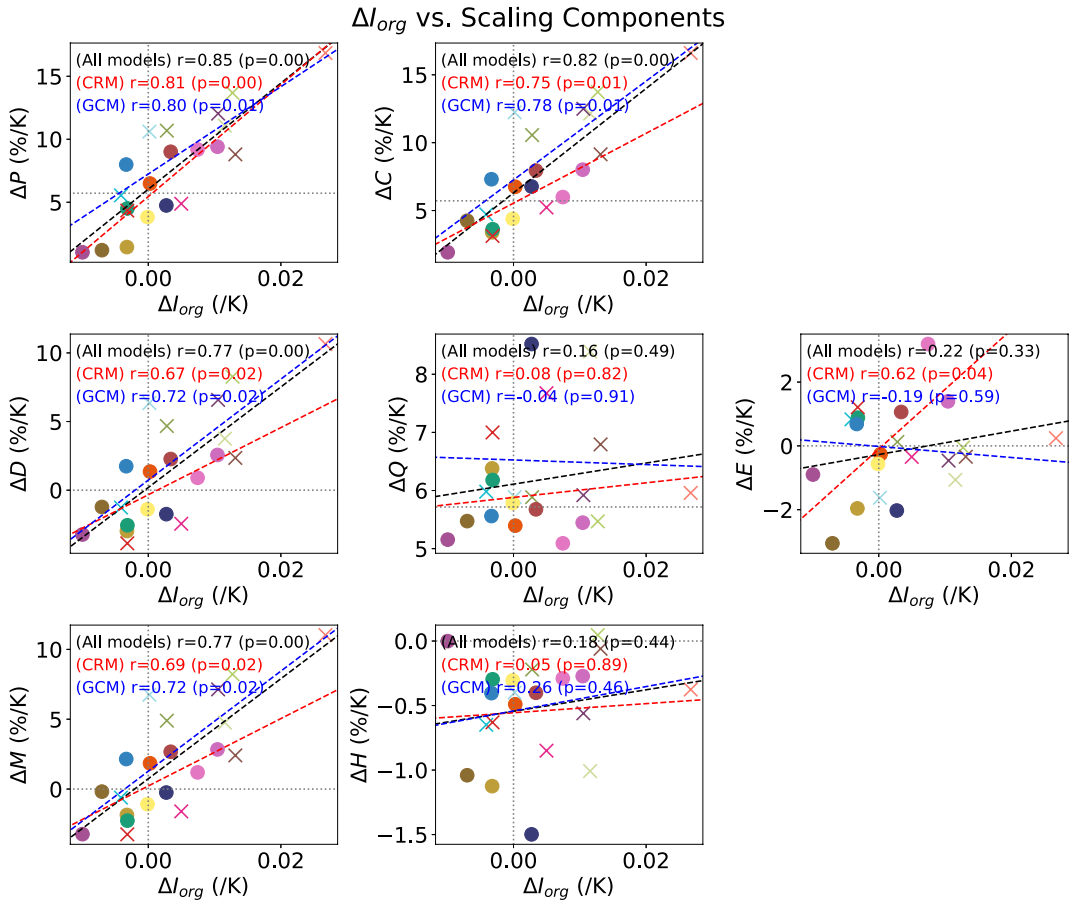

Figure 7. Scaling components for 1-hourly, 15-km precipitation for the large-domain models (defined in Section 2.1) versus the change in organization index. All values are calculated between the 295 and 305 K simulations, and extreme precipitation and scaling components are averaged above the 99.9th percentile. Circles represent CRMs while crosses represent GCMs. The dotted gray vertical lines show no change in organzation. The dotted gray horizontal lines show Clausius-Clapeyron scaling for the components which we expect to scale with SST (ΔP, ΔC, and ΔQ), while they show no change with warming in the other subplots.

restoration of the link between CRH and precipitation efficiency. This suggests the differences between CRMs and GCMs shown here may alternatively be an artifact of the coarser resolution of the GCMs.

Within the dynamic component, changes in the updraft magnitude dominate. The updraft shape component has very little spread and generally results in a tiny negative contribution to ΔP. This is caused by upward movement of the peak updraft with SST warming, into a layer with a smaller saturation moisture lapse rate. As a validation of our shifted-scaling methodology, we also tested correlations involving 99.9th-percentile hourly averaged 15-km 500-hPa vertical velocity (w_{500}) and its changes across CRMs. We find that Δw_{500} has correlation coefficients of 0.77 with ΔP, 0.82 with ΔD, 0.83 with ΔM, and 0.75 with ΔI_{org}. Although these extreme hourly updrafts are not necessarily exactly the same storms as the hourly updrafts associated with 15-km extreme precipitation events, the strong correlations indicate that our results likely would hold if they were conditioned on extreme condensation rather than extreme precipitation. We do not find significant correlations between changes in extreme instantaneous updraft velocity and the scaling components at many levels, consistent with the lack of correlations seen in Figure 5b, although correlations do reach significance for ΔC and Δw from 500 to 800 hPa and for ΔI_{org}, ΔP, and ΔD at 900 hPa (not shown).

5.2. Correlations Between the Scaling Components and Organization

The terms which show large intermodel spreads in Figure 7 are correlated with changes in I_{org}. While ΔI_{org} most strongly correlates with ΔP, it also shows similar statistically significant correlations with ΔC, ΔD, ΔE, and ΔM.

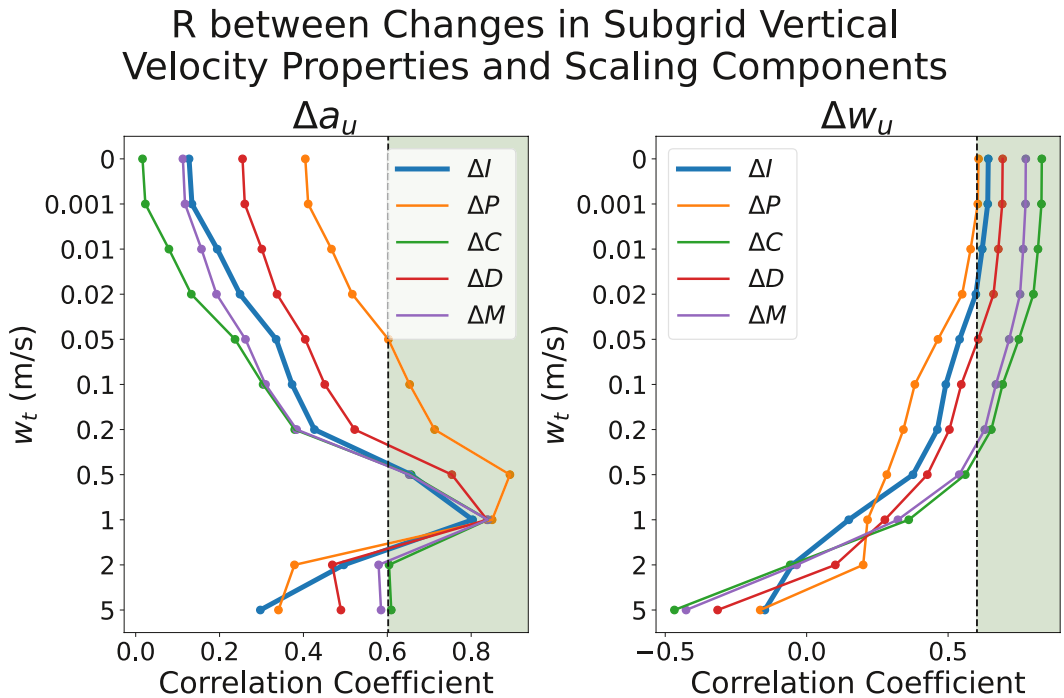

Figure 8. Correlation coefficients between changes in updraft area (a_u) and velocity per unit updraft area (w_u) and ΔI_{org} (blue) and the relevant scaling components (other colors). All scaling components are calculated from the 3-D snapshots before extreme 15-km hourly rainfall, while updraft area and velocity are conditioned on extreme 15-km updrafts. Green shading denotes a statistically significant correlation at p = 0.05.

These suggest primary mechanisms of action of organization on extreme precipitation through updraft magnitude (discussed further in Section 5.3) and precipitation efficiency.

5.3. Understanding the Updraft Magnitude Contribution

As discussed in Section 2.1, the updraft magnitude contribution represents the combined effects of changes in updraft strength and area. To attempt to separate these two effects, we examine the 500 hPa hourly vertical velocity (w_{500}) field across the CRMs without conditioning it on extreme precipitation. As changes in the 99.9th percentile of 1-hourly, 15-km w_{500} show a strong correlation coefficient of r = 0.82 against ΔD, analyzing the two-dimensional updraft velocity field independently of precipitation provides insight into the behavior of updrafts with both a larger sample size and less computation than conditioning three-dimensional updrafts on the occurrence of extreme precipitation. This method also removes any ambiguity related to time-shifting the updrafts relative to the precipitation as we did with the scaling. Within each 15-km hourly updraft extreme (an "extreme box"), we examine statistics of the 3-km grid cells which build it. We can easily extract the updraft area fraction a_u from this by finding the portion of such grid cells which show a positive vertical velocity, or we can choose to define a velocity threshold w_t which must be exceeded to classify a point as an updraft.

$$a_u = \frac{\sum_{w_{500} > w_t} dx\, dy}{\sum dx\, dy} \tag{11}$$

Once we have done so, we can calculate the updraft strength per unit updraft area by dividing the overall $\overline{w_{500}}$ for the extreme box by the updraft area: $w_u = \frac{\overline{w_{500}}}{a_u}$. This analysis parallels Bao et al. (2024)'s examination of the duration of precipitation extremes, but here we examine spatial coverage.

We calculate the rates of change with warming of both a_u and w_u with various values of w_t, and then calculate correlation coefficients between these changes and ΔI_{org}, ΔP, and the relevant scaling components (condensation ΔC, dynamic ΔD, and updraft magnitude ΔM). These correlation coefficients are plotted as a function of w_t in Figure 8.

When we use an updraft threshold of 0 (i.e., any point with a positive vertical velocity is considered an updraft), 60%–90% of each extreme box shows rising motion. However, neither a_u nor Δa_u correlates with I_{org} or its change. As the fractional change in a_u is small, something else must explain the changes in the total updraft mass flux, which is mathematically required to be the "strength" of the updrafts. Given this, it is unsurprising that changes in w_u do correlate with both ΔI and ΔD. This pattern holds for small nonzero updraft thresholds as well.

If we instead choose a larger updraft threshold more representative of convection, we can find drastically different results. A threshold velocity of 1 m/s is more typical of convective cells, so using this threshold may describe both the convective area fraction and a typical convective updraft strength. This threshold is exceeded across 20%–60% of the area of each CRM's extreme boxes at 300 K. Δa_u with this higher threshold is strongly correlated with both ΔI ($r = 0.80$) and ΔD ($r = 0.84$). With this threshold, Δw_u instead does not correlate with either ΔI or ΔD. Care must be taken not to choose a threshold so high that updrafts of that magnitude are rare. Some models struggle to produce frequent updrafts above about 2 m/s, so thresholds larger than this show small updraft area fractions. The result is statistically noisy area changes driven more by variation in how models handle strong updrafts, with a large enough cross-model spread to hide any connection between updraft area and both organization and the components.

Thus, depending on the definition of an updraft, either updraft area fraction or updraft strength could be the factor responsible for the dynamic contribution. We caution that given the nature of real-world updraft ensembles with a spectrum of sizes and strengths, there may be no meaningful difference between changes in size and strength: if updraft strength at each percentile increases, then the area of the updrafts exceeding a given threshold must also increase, and vice versa. However, we overall favor updraft area fraction as the primary driver of the changes in updraft magnitude. An alternative separator of updraft size and strength is the uncoarsened 1-hourly, 3-km case, where there was no significant correlation between either changes in the 99.9th-percentile vertical velocity or ΔD with ΔI (not shown). As the area fraction is necessarily constant at 100% in this uncoarsened case, the dynamic component is controlled solely by updraft strength. The lack of a correlation suggests updraft strength alone does not modulate the link between organization and extreme precipitation. Consistent with the higher thresholds, this suggests updraft area fraction is a major component of the spread in extreme precipitation with warming. This is supported in observations by Schiro et al. (2020), finding that increased precipitation occurs in the same overall environment in MCSs compared to less-organized convection, in part because of the increased area covered by convection.

The result is also consistent with other results which separate the effects of precipitation intensity and spatiotemporal coverage. Roca et al. (2022) find the precipitation area fraction, defined in the same way as we define the updraft area fraction, is the primary driver of coarsened precipitation extremes. Another consistent result is Bao et al. (2024)'s finding that precipitation duration (not intensity) drives the increase in extreme precipitation with increased organization, although we do not find the decreases in intensity found in that study. Both increased duration and increased area reflect an increase in the spatiotemporal extent of the rainfall in extreme precipitation events. However, if we attempt to replicate their precipitation duration and intensity separation directly, we find the same issue as our updraft separation with a low threshold: the duration of rainfall we find is large and changes little, so we do see increases in precipitation "intensity" which may not reflect actual changes in the most intense precipitation extremes (not shown).

5.4. Environmental Variables Linking Organization and Scaling Components

Convective organization is known to have a large impact on its environment, causing a domain-mean warming and drying, with a vertical profile closer to a moist adiabat (Wing & Cronin, 2016). The convecting region also warms but shows moistening. In this section, we examine which environmental variables modulated by organization may contribute to enhanced extreme precipitation via the dynamic and efficiency terms.

5.4.1. CAPE

If convective organization modulates updraft strength, CAPE is a reasonable variable to investigate as the conversion of CAPE to kinetic energy places an upper bound on updraft strength. We investigate how CAPE, as calculated from the local surface parcel and environment an hour before the onset of an extreme precipitation event, relates to organization. Notice how this is an additional hour before we calculate the scaling components: we must look earlier to remove the effect of existing updrafts, and use this additional hour of shifting to represent

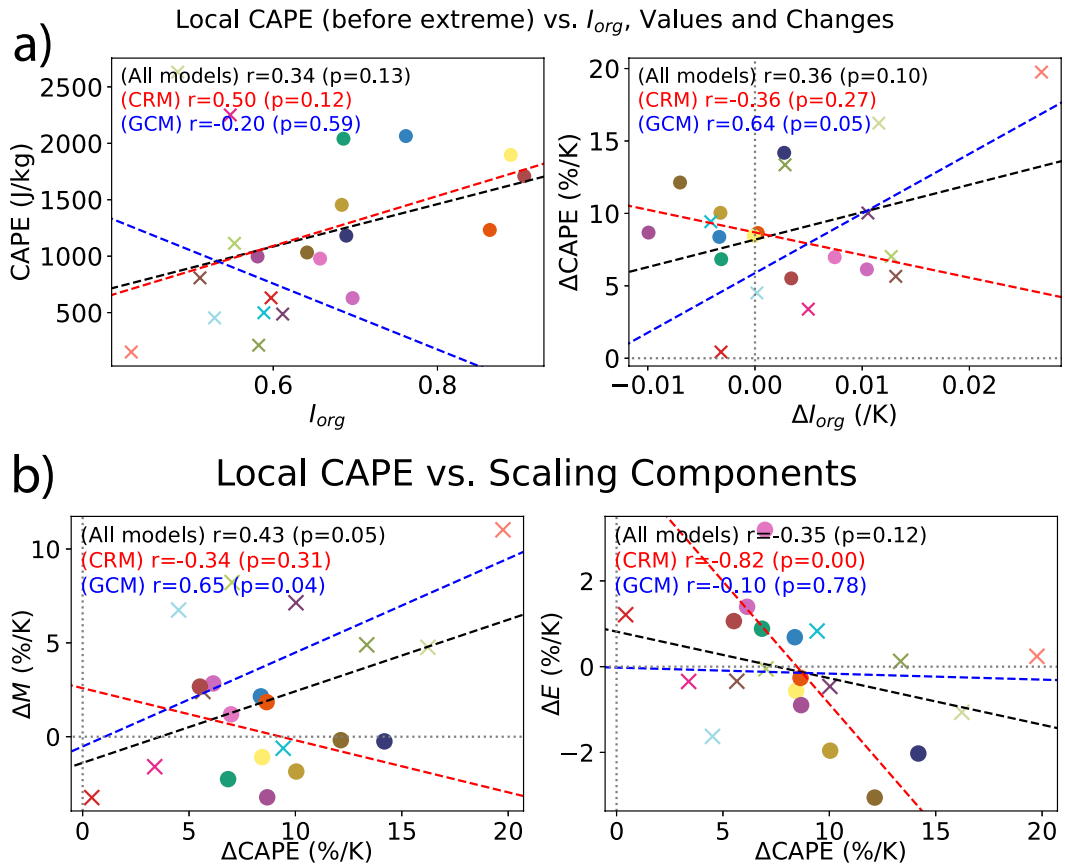

Figure 9. (a) Relationship between CAPE, calculated using the lowest-layer parcel and local environmental profile conditioned on extreme precipitation, and organization index in the large-domain simulations. Values at 300 K (left) and changes between 295 and 305 K (right) are shown. (b) Correlations between CAPE changes and the updraft magnitude and efficiency scaling components between 295 and 305 K. CAPE is calculated before a precipitation extreme at 15-km resolution.

the environment in which convection initiates. Although physically relevant, it does not appear that the exact time shift chosen dramatically influences the results: we examined the environments from 3 hr before onset of extreme precipitation to 1 hr after it finishes, finding little qualitative change as long as CAPE is calculated before extreme precipitation occurs. When the extra shift is performed, Figure 9a shows a positive correlation between CAPE and I_{org} across CRMs, but a correlation of the opposite sign when considering changes with warming. However, Figure 9b shows CAPE does not significantly correlate with ΔM, and is strongly negatively correlated with ΔE. The lack of a correlation between CAPE and ΔM generally agrees with Singh and O'Gorman (2015), finding that CAPE increases far more rapidly with warming than updraft magnitude due to the influence of entrainment. CAPE and precipitation efficiency have been theoretically linked: according to the analytic theory of Romps (2016), if precipitation efficiency is treated as an external parameter, its increases should result in higher CAPE. This is the inverse of the correlation we see here. However, changes in CAPE with warming across RCEMIP's small-domain simulations are not driven by cross-model variations in efficiency (Wing & Singh, 2024). Considering the mixed signals in how CAPE relates with organization index, we suspect the negative relationship between CAPE and efficiency is a correlation without a direct causation, linked instead by their mutual correlation with organization. This demonstrates the dangers of looking for causal effects on precipitation changes across models when there is known to be another linking factor, and suggests even strong correlations may be spurious here.

Under quasi-equilibrium in the RCE state, CAPE is more of an emergent property of a continuously convecting environment than a predictor of updraft strength (Arakawa & Schubert, 1974; Emanuel et al., 1994; Singh & O'Gorman, 2013). The right panel of Figure 9a hints that the decrease in CAPE with increasing organization may

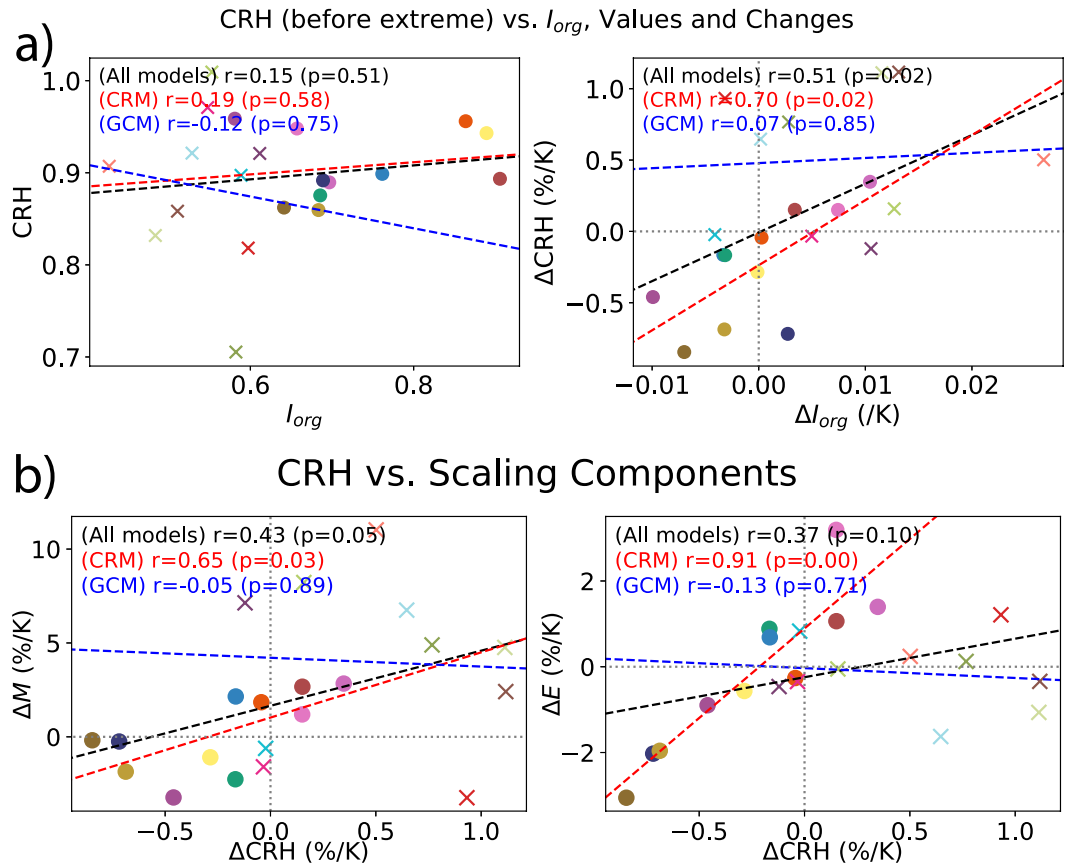

Figure 10. (a) Relationship between CRH and organization index in the large-domain simulations. Values at 300 K (left) and changes between 295 and 305 K (right) are shown. (b) Correlations between CRH changes and the dynamic and efficiency scaling components in the large-domain simulations. CRH changes and scaling components are calculated between 295 and 305 K at 15-km resolution. Both are calculated at the beginning of an hourly precipitation extreme.

reflect an environmental property, namely, the warming and moistening with organization seen in the moist region. This moistening could itself impact extreme precipitation, as demonstrated in the next section.

5.4.2. Column Relative Humidity

As a measure of moisture in the convecting region, we examine column relative humidity (CRH), conditional on the beginning of an extreme precipitation event. Organization increases the contrast in moisture between the wet and dry regions, and while this primarily manifests as a drying of the dry region, the convecting region is also moistened. As with CAPE, we examined several time shifts of the environment relative to extreme precipitation, and found that the choice of conditioning CRH on the time of extreme precipitation's onset qualitatively makes little difference, though correlations are somewhat stronger if the CRH is calculated temporally closer to the extreme precipitation events. Although no correlation is seen between the value of CRH and the value of I_{org} in Figure 10a, a significant correlation exists between changes in CRH and changes in I_{org} in CRMs. This correlation is robust to both percentile and organization metric, as changes in CRH also correlate with changes in subsidence fraction.

Changes in CRH correlate extremely well with the efficiency contribution in CRMs while also correlating with the dynamic contribution (Figure 10b). Both correlations are strong for 15-km resolution, but when further coarsened to 60 km, the correlation between ΔI_{org} and ΔD becomes stronger (r = 0.80) while the correlation between ΔI_{org} and ΔE weakens (r = 0.80) (not shown). In both the 15 and 60-km cases, ΔCRH correlates more strongly with each of these scaling components than it does with ΔI_{org}, which is consistent with ΔCRH being a pathway through which organization can influence the scaling components. However, the lack of a correlation

between the value of CRH and the value of I_{org} and the lack of comparable correlations across the GCMs imply it cannot be the only such pathway.

We investigated the relationship between the dynamic and efficiency components and CRH calculated both at the beginning and at the end of an extreme precipitation event. One might expect the ΔCRH-ΔD correlation to be more-dependent on the pre-precipitation environment (the environment encountered by a rising parcel) while the ΔCRH-ΔE could depend more on the post-precipitation environment (the environment encountered and modified by falling hydrometeors). However, we find that the CRH is similar before and after extreme precipitation, with similar resulting correlation coefficients at both times.

The relationship between ΔCRH and ΔE could most easily be explained by reduced re-evaporation of hydrometeors in a more humid environment. The dynamic contribution is more difficult to attribute. One theory on how environmental moisture impacts convective updrafts is that entrainment of moister air causes less reduction of buoyancy (Singh & O'Gorman, 2015). An alternative theory is that a more humid environment reduces the MSE difference between the free troposphere and the boundary layer, requiring more downdraft flux (and compensating updraft flux) to balance surface energy fluxes in boundary-layer quasi-equilibrium (Emanuel, 2019). It is also possible that the dynamic component and CRH are correlated without a causal pathway, simply because of their mutual correlations with the degree of organization. We next examine MSE in hopes of understanding which of these theories may apply.

5.4.3. MSE-Related Variables

For another perspective on how changes in organization impact extreme precipitation, we examined moist static energy $h = c_pT + gz + L_vq$, as well as saturated MSE $h^* = c_pT + gz + L_vq_s$ and the saturation deficit $h^* - h$. Saturation MSE effectively shows the importance of temperature, while the saturation deficit acts as a measure of dryness. We examined the vertical structure of the correlations between changes in organization, the organization-related scaling components, and each of these MSE variables by calculating the average MSE (in J/kg) in each 100-hPa-thick layer of the atmosphere, as well as the total atmosphere from 100 to 1,000 hPa. Results are graphed in Figure 11.

As with CRH, the value of each of these variables does not significantly correlate with I_{org} (not shown), but the changes in the MSE variables do correlate with ΔI_{org} at most levels. There is a statistically significant correlation between ΔI_{org} and Δh at all layers above the boundary layer, with hints of a correlation in the near-surface layer. Changes in h also correlate with the changes in precipitation in all layers, which appears to be dominated by the efficiency component. In the tropics, variability of moisture dominates MSE variability, so it makes sense that correlations seen here agree with those seen in the previous section: changes in MSE are sensitive to the same variable that changes CRH.

Saturation MSE (h^*) instead focuses on temperature, removing the effect of varying moisture. The results are still broadly similar to those seen with h, largely because environments which support extreme precipitation tend to be near saturation. As with h, there are stronger correlations between h^*, ΔI_{org}, and the scaling components when h^* is examined higher in the troposphere. The correlation between Δh^* and ΔI_{org} implies that organization warms the upper troposphere, as expected if rising parcels remain closer to a moist adiabat while being lifted. This could itself be a symptom of the entrainment of moister air causing a reduction of buoyancy loss in updrafts, which could explain why the Δh^*-ΔD correlation strengthens with height. By contrast, the correlation between Δh^* and ΔE is notably weaker than the correlation between Δh and ΔE, suggesting it is instead the moisture component of MSE connecting organization to precipitation efficiency.

We choose not to plot the saturation deficit in Figure 11. As the atmosphere surrounding an extreme precipitation event can experience supersaturation, the saturation deficit sometimes becomes negative, resulting in non-physical rates of change and extreme outliers making any correlations meaningless. However, when integrating over the entire column, we find statistically significant negative correlations between changes in column-integrated saturation deficit and I_{org} and the scaling components. This result is to be expected, as column-integrated saturation deficit is effectively a measure of CRH, described in Section 5.4.2.

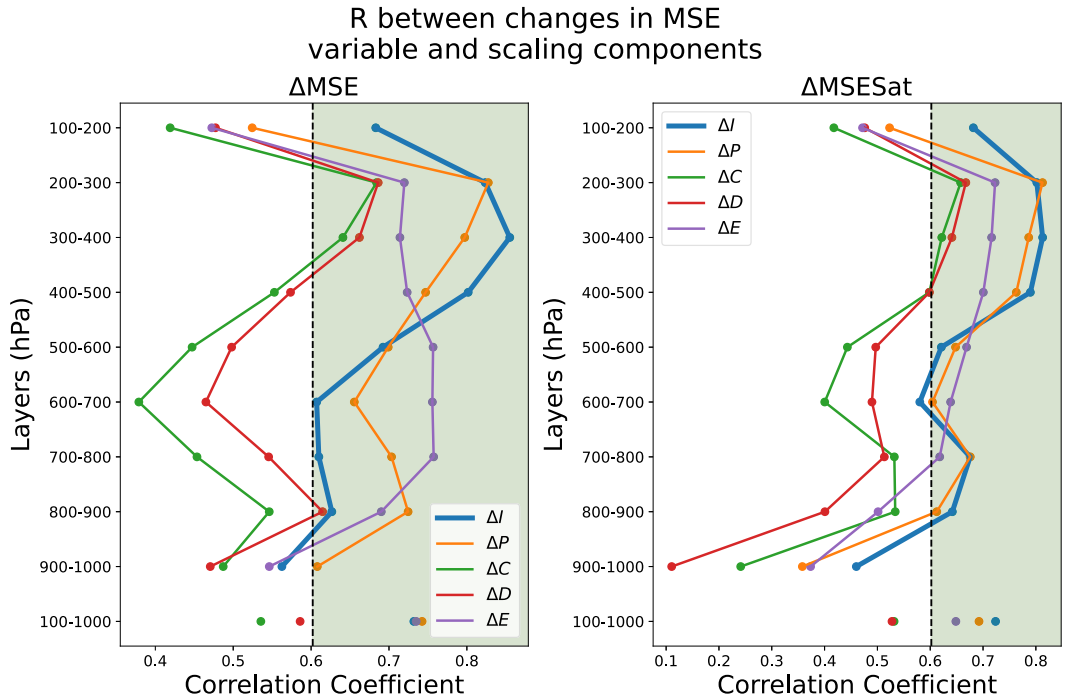

Figure 11. Correlation coefficients between changes in MSE and saturation MSE calculated within the given layers and ΔI_{org} (blue) and the relevant scaling components (other colors). The 100–1,000 hPa layer represents the full troposphere. All variables are calculated from the 3-D snapshots before extreme 15-km hourly rainfall across CRMs. Green shading denotes a statistically significant correlation at p = 0.05.

5.5. Comparison of CRM and GCM Results

The previous section primarily focused on relationships between organization and extreme precipitation across the CRMs of the RCEMIP ensemble. Comparing these results to the GCMs provides added context to our CRM results, highlighting what we can learn from RCEMIP that prior GCM-based studies may have been unable to find and proving which results are robust. Compared to CRMs, the GCMs are analyzed at coarser resolutions, and show larger variation in the dynamic contribution but smaller variation in the implied efficiency contribution (Figure 6). Like the CRMs, the GCMs show correlations between ΔI_{org} and several scaling components, namely precipitation, condensation, dynamic, and magnitude (Figure 7). Notably, the correlation between ΔI_{org} and ΔE is lost. As all three correlations between pairs of ΔI_{org}, ΔE, and ΔCRH are present in CRMs but absent in GCMs, this suggests the CRMs are able to capture an environmental factor contributing to changes in extreme precipitation that the GCMs are unable to represent through their parameterizations. We hypothesize that this involves the convective parameterization. Eight of the 10 GCMs examined- specifically those which do not use super-parameterization- output their convective precipitation P_c. In four of these, P_c comprises nearly all of the total extreme precipitation, while in the other four approximately half of the total comes from the parameterization. ΔP_c correlates strongly with both ΔP (r = 0.87) and ΔM (r = 0.82) while remaining completely uncorrelated with ΔE (r = −0.07), suggesting that the convectively driven extreme precipitation events in the GCMs are unaffected by precipitation efficiency. If the convective parameterization includes instantaneous fallout of precipitation, then this precipitation would not experience the moister environment of the organized region, breaking the links between ΔP, ΔE, and ΔCRH seen in the CRMs.

On the updraft magnitude contribution, we still see correlations between ΔI_{org} and ΔM across the GCMs, but correlations involving both of these and ΔCRH are lost. This implies the link between organization and updraft magnitude is not modulated by moisture in the GCMs, but some other environmental variable must still link them as the GCMs are unable to explicitly represent the convective updraft packing seen in the CRMs. It also may suggest the link between changes in moisture and updraft magnitude in the CRMs could simply represent their mutual correlations with the change in organization.

We also note that many correlations seen in the GCMs are not statistically robust. One model (GEOS-GCM) is an outlier in both its changes in organization and extreme precipitation. If this model is excluded from the analysis, the correlations between ΔI_{org} and the scaling components of ΔP, ΔD, and ΔM all lose significance at the $p = 0.05$ level. While the ΔI_{org}-ΔC correlation remains barely significant, and the I_{org}-ΔP correlation is only just insignificant ($p = 0.052$), the lack of any correlations involving the dynamic, thermodynamic, and efficiency terms shows that if we remove this model from the analysis, we are unable to extract physical mechanisms for the relationship between changes in extreme precipitation and changes in organization by using the scaling framework.

6. Conclusions

The presence of organized convection dramatically increases precipitation extremes across models in an RCE configuration. Within simulations that permit organization, changes in the degree of organization with warming correlate with changes in extreme precipitation across a wide range of spatiotemporal scales. Although these changes are most strongly correlated on subdaily timescales on the mesoscale, significant correlations are seen down to 6-km spatial resolution and hourly precipitation. Compared against the organization-forbidding small-domain simulations, the presence of organized convection appears to amplify even 3-km rainfall at sufficiently long timescales and instantaneous precipitation over sufficiently large regions. Organization modulates extreme precipitation via changes in the updraft magnitudes leading to extreme condensation events and via the microphysical processes linking condensation and precipitation rates. Both mechanisms could be explained by the high column relative humidity present in the organized region, which could act through reduced buoyancy loss through entrainment (Singh & O'Gorman, 2015), greater downdraft flux into the boundary layer (Emanuel, 2019), and reduced re-evaporation. However, due to limits of the RCEMIP data set, it is difficult to causally attribute changes in extreme precipitation to any of these mechanisms. Changes in updraft magnitude specifically may be explained simply due to increased spatial coherence of convective updrafts in a more organized scene. It is also unclear whether 3-km resolution is truly sufficient to resolve all relevant processes to modulation of extreme precipitation, as it is still comparable to the scale of convective cells. Regardless of the responsible mechanism, this analysis proves that changes in the degree of convective organization are clearly a primary factor in determining how extreme precipitation rates change with warming, and demonstrates that finer model resolutions may help clarify prior disagreements on how extreme precipitation may change with warming from GCM studies. Our results are generally consistent with prior studies, but by leveraging an ensemble of CRMs from RCEMIP this is the most comprehensive analysis to date. Clearly, accurately modeling convective organization is crucial to predicting the impacts of extreme rainfall both now and with future climate change.

RCEMIP phase II (Wing et al., 2024) will soon be available and will introduce SST gradients to the simulations. These mock-Walker simulations will allow examination of precipitation extremes and organized convection under more realistic conditions, including an SST-forced circulation in addition to the self-aggregation-induced circulations.

Acknowledgments
Funding for this project was provided by NSF Grant AGS 2140419. Python code for processing RCEMIP data was originally written by Catherine Stauffer. Python code for calculating the scaling was borrowed from Oliver Angelil, translated from MATLAB code originally by Paul O'Gorman. Code for calculating CAPE was translated from MATLAB code written by Allison A. Wing and Martin S. Singh. Additional thanks to all RCEMIP contributors for running the simulations and to the German Climate Computing Center (DKRZ) for hosting RCEMIP data, which is publicly available at http://hdl.handle.net/21.14101/d4beee8e-6996-453e-bbd1-ff53b6874c0e. The authors would also like to thank two anonymous reviewers for their contributions in improving this paper.

Data Availability Statement

The standardized RCEMIP data (Wing et al., 2020b) is hosted by the German Climate Computing Center (DKRZ) and is publicly available online at http://hdl.handle.net/21.14101/d4beee8e-6996-453e-bbd1-ff53b6874c0e. Other data derived from RCEMIP for this study and the analysis scripts are in a Zenodo repository at http://doi.org/10.5281/zenodo.12549358 (O'Donnell & Wing, 2024).

References

Abbott, T. H., Cronin, T. W., & Beucler, T. (2020). Convective dynamics and the response of precipitation extremes to warming in radiative–convective equilibrium. *Journal of the Atmospheric Sciences*, *77*(5), 1637–1660. https://doi.org/10.1175/JAS-D-19-0197.1

Abramian, S., Muller, C. J., & Risi, C. (2023). Extreme precipitation in tropical squall lines. *Journal of Advances in Modeling Earth Systems*, *15*(10), e2022MS003477. https://doi.org/10.1029/2022MS003477

Allen, M. R., & Ingram, W. J. (2002). Constraints on future changes in climate and the hydrologic cycle. *Nature*, *419*(6903), 228–232. https://doi.org/10.1038/nature01092

Arakawa, A., & Schubert, W. H. (1974). Interaction of a cumulus cloud ensemble with the large-scale environment, part I. *Journal of the Atmospheric Sciences*, *31*(3), 674–701. https://doi.org/10.1175/1520-0469(1974)031<0674:ioacce>2.0.co;2

Bao, J., & Sherwood, S. C. (2019). The role of convective self-aggregation in extreme instantaneous versus daily precipitation. *Journal of Advances in Modeling Earth Systems*, *11*(1), 19–33. https://doi.org/10.1029/2018MS001503

Bao, J., Sherwood, S. C., Colin, M., & Dixit, V. (2017). The robust relationship between extreme precipitation and convective organization in idealized numerical modeling simulations. *Journal of Advances in Modeling Earth Systems*, *9*(6), 2291–2303. https://doi.org/10.1002/2017MS001125

Bao, J., Stevens, B., Kluft, L., & Muller, C. J. (2024). Intensification of daily tropical precipitation extremes from more organized convection. *Science Advances*, *10*(8), eadj6801. https://doi.org/10.1126/sciadv.adj6801

Becker, T., & Wing, A. A. (2020). Understanding the extreme spread in climate sensitivity within the Radiative-Convective Equilibrium Model Intercomparison Project. *Journal of Advances in Modeling Earth Systems*, *12*(10), e2020MS002165. https://doi.org/10.1029/2020MS002165

Dai, N., & Soden, B. J. (2020). Convective aggregation and the amplification of tropical precipitation extremes. *AGU Advances*, *1*(4), e2020AV000201. https://doi.org/10.1029/2020AV000201

Da Silva, N. A., Muller, C. J., Shamekh, S., & Fildier, B. (2021). Significant amplification of instantaneous extreme precipitation with convective self-aggregation. *Journal of Advances in Modeling Earth Systems*, *13*(11). https://doi.org/10.1029/2021MS002607

Emanuel, K. (2019). Inferences from simple models of slow, convectively coupled processes. *Journal of the Atmospheric Sciences*, *76*(1), 195–208. https://doi.org/10.1175/JAS-D-18-0090.1

Emanuel, K., Neelin, J. D., & Bretherton, C. S. (1994). On large-scale circulations in convecting atmospheres. *Quarterly Journal of the Royal Meteorological Society*, *120*(519), 1111–1143. https://doi.org/10.1002/qj.49712051902

Fildier, B., Collins, W. D., & Muller, C. J. (2021). Distortions of the rain distribution with warming, with and without self-aggregation. *Journal of Advances in Modeling Earth Systems*, *13*(2), e2020MS002256. https://doi.org/10.1029/2020MS002256

Fildier, B., Parishani, H., & Collins, W. D. (2017). Simultaneous characterization of mesoscale and convective-scale tropical rainfall extremes and their dynamical and thermodynamic modes of change. *Journal of Advances in Modeling Earth Systems*, *9*(5), 2103–2119. https://doi.org/10.1002/2017MS001033

Hamada, A., Murayama, Y., & Takayabu, Y. N. (2014). Regional characteristics of extreme rainfall extracted from TRMM PR measurements. *Journal of Climate*, *27*(21), 8151–8169. https://doi.org/10.1175/JCLI-D-14-00107.1

Li, R. L., Studholme, J. H. P., Fedorov, A. V., & Storelvmo, T. (2022). Precipitation efficiency constraint on climate change. *Nature Climate Change*, *12*(7), 642–648. https://doi.org/10.1038/s41558-022-01400-x

Lutsko, N. J., & Cronin, T. W. (2018). Increase in precipitation efficiency with surface warming in radiative-convective equilibrium. *Journal of Advances in Modeling Earth Systems*, *10*(11), 2992–3010. https://doi.org/10.1029/2018MS001482

Medeiros, B., Clement, A. C., Benedict, J. J., & Zhang, B. (2021). Investigating the impact of cloud-radiative feedbacks on tropical precipitation extremes. *Npj Climate and Atmospheric Science*, *4*(1), 1–10. https://doi.org/10.1038/s41612-021-00174-x

Muller, C. J. (2013). Impact of convective organization on the response of tropical precipitation extremes to warming. *Journal of Climate*, *26*(14), 5028–5043. https://doi.org/10.1175/JCLI-D-12-00655.1

Muller, C. J., O'Gorman, P. A., & Back, L. E. (2011). Intensification of precipitation extremes with warming in a cloud-resolving model. *Journal of Climate*, *24*(11), 2784–2800. https://doi.org/10.1175/2011JCLI3876.1

Muller, C. J., & Takayabu, Y. (2020). Response of precipitation extremes to warming: What have we learned from theory and idealized cloud-resolving simulations, and what remains to be learned? *Environmental Research Letters*, *15*(3), 035001. https://doi.org/10.1088/1748-9326/ab7130

Nesbitt, S. W., Cifelli, R., & Rutledge, S. A. (2006). Storm morphology and rainfall characteristics of TRMM precipitation features. *Monthly Weather Review*, *134*(10), 2702–2721. https://doi.org/10.1175/MWR3200.1

Nikumbh, A. C., Lin, P., Paynter, D., & Ming, Y. (2024). Does increasing horizontal resolution improve the simulation of intense tropical rainfall in GFDL's AM4 model? *Geophysical Research Letters*, *51*(12), e2023GL106708. https://doi.org/10.1029/2023GL106708

O'Donnell, G. L., & Wing, A. A. (2024). Precipitation extremes in RCEMIP: Code and derived data. *Zenodo*. https://doi.org/10.5281/zenodo.12549358

O'Gorman, P. A. (2012). Sensitivity of tropical precipitation extremes to climate change. *Nature Geoscience*, *5*(10), 697–700. https://doi.org/10.1038/ngeo1568

O'Gorman, P. A. (2015). Precipitation extremes under climate change. *Current Climate Change Reports*, *1*(2), 49–59. https://doi.org/10.1007/s40641-015-0009-3

O'Gorman, P. A., & Schneider, T. (2009a). The physical basis for increases in precipitation extremes in simulations of 21st-century climate change. *Proceedings of the National Academy of Sciences of the United States of America*, *106*(35), 14773–14777. https://doi.org/10.1073/pnas.0907610106

O'Gorman, P. A., & Schneider, T. (2009b). Scaling of precipitation extremes over a wide range of climates simulated with an idealized GCM. *Journal of Climate*, *22*(21), 5676–5685. https://doi.org/10.1175/2009JCLI2701.1

Parodi, A., & Emanuel, K. (2009). A theory for buoyancy and velocity scales in deep moist convection. *Journal of the Atmospheric Sciences*, *66*(11), 3449–3463. https://doi.org/10.1175/2009JAS3103.1

Pendergrass, A. G. (2020). Changing degree of convective organization as a mechanism for dynamic changes in extreme precipitation. *Current Climate Change Reports*, *6*(2), 47–54. https://doi.org/10.1007/s40641-020-00157-9

Pendergrass, A. G., Reed, K. A., & Medeiros, B. (2016). The link between extreme precipitation and convective organization in a warming climate: Global radiative-convective equilibrium simulations. *Geophysical Research Letters*, *43*(21), 11445–11452. https://doi.org/10.1002/2016GL071285

Rios-Berrios, R., Bryan, G. H., Medeiros, B., Judt, F., & Wang, W. (2022). Differences in tropical rainfall in aquaplanet simulations with resolved or parameterized deep convection. *Journal of Advances in Modeling Earth Systems*, *14*(5), e2021MS002902. https://doi.org/10.1029/2021MS002902

Roca, R., De Meyer, V., & Muller, C. (2022). Precipitating fraction, not intensity, explains extreme coarse-grained precipitation Clausius-Clapeyron scaling with sea surface temperature over tropical oceans. *Geophysical Research Letters*, *49*(24), e2022GL100624. https://doi.org/10.1029/2022GL100624

Roca, R., & Fiolleau, T. (2020). Extreme precipitation in the tropics is closely associated with long-lived convective systems. *Communications Earth & Environment*, *1*(1), 1–6. https://doi.org/10.1038/s43247-020-00015-4

Romps, D. M. (2011). Response of tropical precipitation to global warming. *Journal of the Atmospheric Sciences*, *68*(1), 123–138. https://doi.org/10.1175/2010JAS3542.1

Romps, D. M. (2016). Clausius–Clapeyron scaling of CAPE from analytical solutions to RCE. *Journal of the Atmospheric Sciences*, *73*(9), 3719–3737. https://doi.org/10.1175/JAS-D-15-0327.1

Schär, C., Ban, N., Fischer, E. M., Rajczak, J., Schmidli, J., Frei, C., et al. (2016). Percentile indices for assessing changes in heavy precipitation events. *Climatic Change*, *137*(1), 201–216. https://doi.org/10.1007/s10584-016-1669-2

Schiro, K. A., Sullivan, S. C., Kuo, Y.-H., Su, H., Gentine, P., Elsaesser, G. S., et al. (2020). Environmental controls on tropical mesoscale convective system precipitation intensity. *Journal of the Atmospheric Sciences*, *77*(12), 4233–4249. https://doi.org/10.1175/JAS-D-20-0111.1

Semie, A. G., & Bony, S. (2020). Relationship between precipitation extremes and convective organization inferred from satellite observations. *Geophysical Research Letters*, *47*(9), e2019GL086927. https://doi.org/10.1029/2019GL086927

Singh, M. S., & O'Gorman, P. A. (2013). Influence of entrainment on the thermal stratification in simulations of radiative-convective equilibrium. *Geophysical Research Letters*, *40*(16), 4398–4403. https://doi.org/10.1002/grl.50796

Singh, M. S., & O'Gorman, P. A. (2014). Influence of microphysics on the scaling of precipitation extremes with temperature. *Geophysical Research Letters*, *41*(16), 6037–6044. https://doi.org/10.1002/2014GL061222

Singh, M. S., & O'Gorman, P. A. (2015). Increases in moist-convective updraught velocities with warming in radiative-convective equilibrium: Increases in updraught velocities with warming. *Quarterly Journal of the Royal Meteorological Society*, *141*(692), 2828–2838. https://doi.org/10.1002/qj.2567

Terai, C. R., Caldwell, P. M., Klein, S. A., Tang, Q., & Branstetter, M. L. (2018). The atmospheric hydrologic cycle in the ACME v0.3 model. *Climate Dynamics*, *50*(9), 3251–3279. https://doi.org/10.1007/s00382-017-3803-x

Tompkins, A. M., & Semie, A. G. (2017). Organization of tropical convection in low vertical wind shears: Role of updraft entrainment. *Journal of Advances in Modeling Earth Systems*, *9*(2), 1046–1068. https://doi.org/10.1002/2016MS000802

Westra, S., Fowler, H. J., Evans, J. P., Alexander, L. V., Berg, P., Johnson, F., et al. (2014). Future changes to the intensity and frequency of short-duration extreme rainfall. *Reviews of Geophysics*, *52*(3), 522–555. https://doi.org/10.1002/2014RG000464

Wing, A. A. (2019). Self-aggregation of deep convection and its implications for climate. *Current Climate Change Reports*, *5*, 1–11. https://doi.org/10.1007/s40641-019-00120-3

Wing, A. A., & Cronin, T. W. (2016). Self-aggregation of convection in long channel geometry. *Quarterly Journal of the Royal Meteorological Society*, *142*(694), 1–15. https://doi.org/10.1002/qj.2628

Wing, A. A., Reed, K. A., Satoh, M., Stevens, B., Bony, S., & Ohno, T. (2018). Radiative–convective equilibrium model intercomparison project. *Geoscientific Model Development*, *11*(2), 793–813. https://doi.org/10.5194/gmd-11-793-2018

Wing, A. A., Silvers, L. G., & Reed, K. A. (2024). RCEMIP-II: Mock-Walker simulations as phase II of the radiative–convective equilibrium model intercomparison project. *Geoscientific Model Development*, *17*(16), 6195–6225. https://doi.org/10.5194/gmd-17-6195-2024

Wing, A. A., & Singh, M. S. (2024). Control of stability and relative humidity in the Radiative-Convective Equilibrium Model Intercomparison Project. *Journal of Advances in Modeling Earth Systems*, *16*(1), e2023MS003914. https://doi.org/10.1029/2023MS003914

Wing, A. A., Stauffer, C. L., Becker, T., Reed, K. A., Ahn, M.-S., Arnold, N. P., et al. (2020a). Clouds and convective self-aggregation in a multimodel ensemble of radiative-convective equilibrium simulations. *Journal of Advances in Modeling Earth Systems*, *12*(9), e2020MS002138. https://doi.org/10.1029/2020MS002138

Wing, A. A., Stauffer, C. L., Becker, T., Reed, K. A., Ahn, M.-S., Arnold, N. P., et al. (2020b). Radiative-Convective Equilibrium Model Intercomparison Project (RCEMIP) simulation dataset. *WDC Climate*. Retrieved from http://hdl.handle.net/21.14101/d4beee8e-6996-453e-bbd1-ff53b6874c0e